Supporting Information for

The Evolution of Anionic Nanoclusters at the Electrode Interface in Water-in-salt Electrolytes

*Lei Zhang[1,3†], Yuanxi Yu[2,3†], Liumin Suo[4], Wei Zhuang[5], Lunhua He[6], Xiaohua Zhang[*7], Liang Hong[*2,3], Pan Tan[*3]*

1. School of Materials and Science Engineering, Shanghai Jiao Tong University, Shanghai 200240, China.
2. School of Physics and Astronomy, Shanghai Jiao Tong University, Shanghai 200240, China.
3. Institute of Natural Sciences, Shanghai Jiao Tong University, Shanghai 200240, China.
4. Beijing Advanced Innovation Center for Materials Genome Engineering, Key Laboratory for Renewable Energy, Beijing Key Laboratory for New Energy Materials and Devices, Beijing National Laboratory for Condensed Matter Physics, Institute of Physics, Chinese Academy of Sciences, Beijing 100190, China.
5. Fujian Institute of Research on the Structure of Matter, Chinese Academy of Sciences Fuzhou, Fujian 350002, China
6. Beijing National Laboratory for Condensed Matter Physics, Institute of Physics, Chinese Academy of Sciences, Beijing 100190, China; Spallation Neutron Source Science Center, Dongguan 523803, China.
7. School of Physical Science and Technology, and Center for Soft Condensed Matter Physics and Interdisciplinary Research, Soochow University, Suzhou 215006, China

†These authors contributed equally to this work

*Email: zhangxiaohua@suda.edu.cn; hongl3liang@sjtu.edu.cn; tpan1039@sjtu.edu.cn

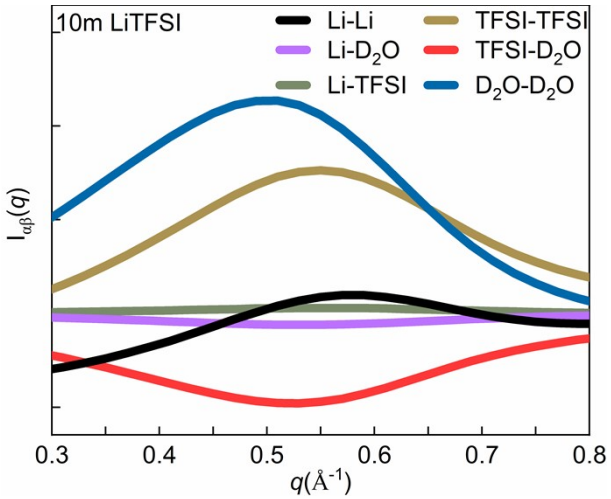

Figure S1. Partial neutron scattering profile (PNSP) of different pairs derived from MD with Model 1 in 10 m LiTFSI electrolyte.

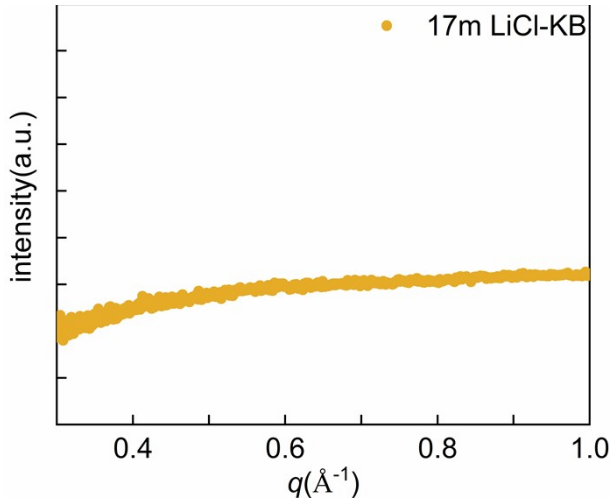

Figure S2. The neutron diffraction for 17 m LiCl electrolyte.

As shown in Figure S3, the enlarged distances (d_2 and $d_3 > d_1$) occur with decreasing salt concentration and the introduction of the KB electrode. However, the mechanisms behind it are different. For LiTFSI electrolyte concentration, the larger distance is attributed to the presence of more water molecules between the adjacent anionic nanoclusters. For the KB electrode, the anionic nanoclusters aggregate to form the larger size of clusters near the interface due to the cation-π interaction. Meanwhile, these two models are similar to the results of the literature, which is the reason that causes the shift peaks are different for the two types of WiSEs.[1]

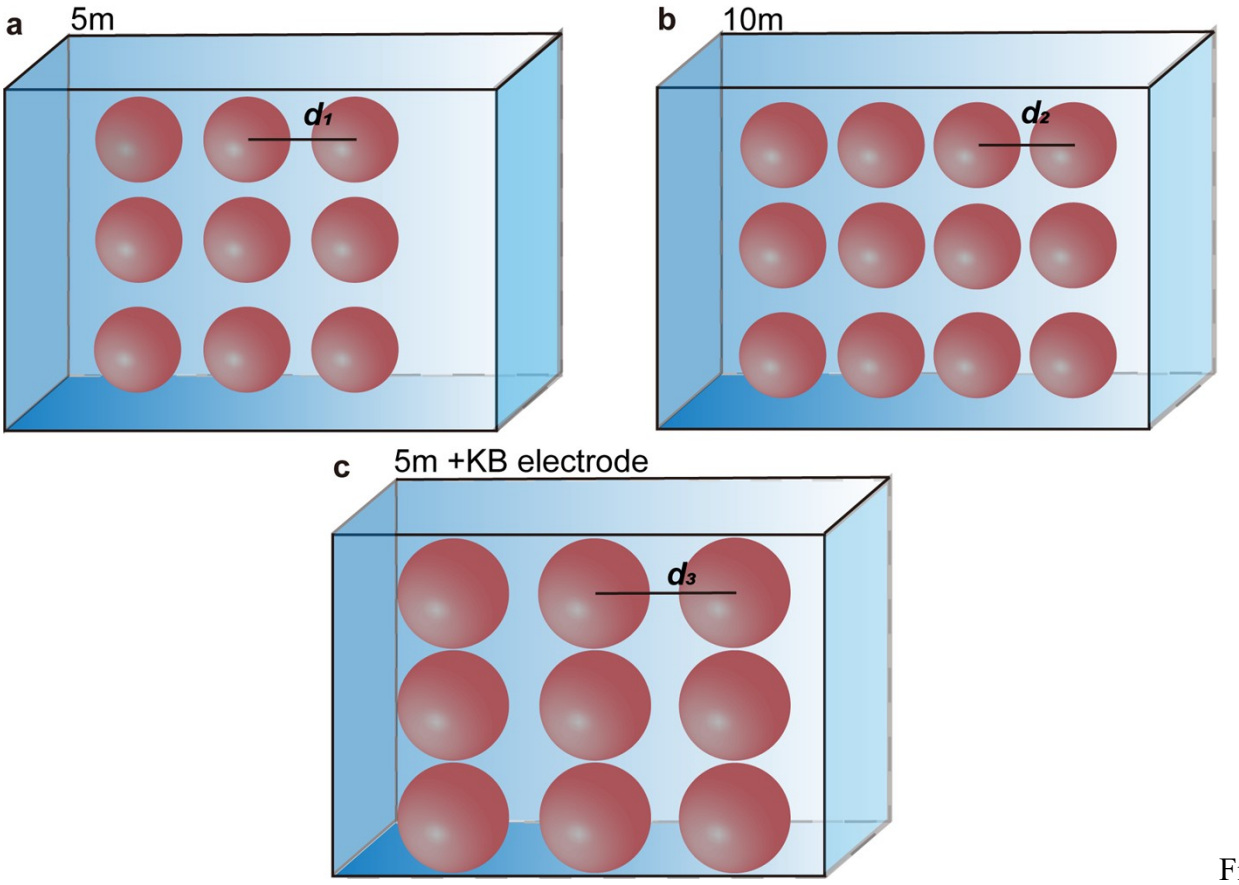

Figure S3. The schematic diagram of the distance changes with varying salt concentrations and with the KB electrode introduction. (a) 5 m LiTFSI; (b) 10 m LiTFSI; (c) 5 m LiTFSI with KB electrodes.

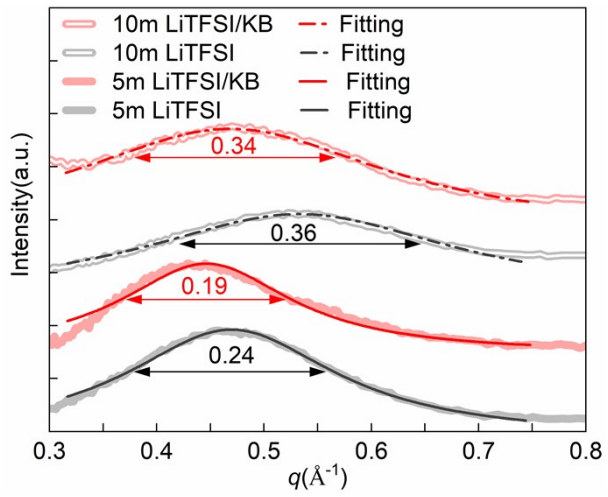

Figure S4. The characteristic peak of LiTFSI electrolyte in neutron diffraction: 5 m with (red line) and without (black line) the KB electrode, 10 m with (red hollow line) and without (black hollow line) the KB electrode, and the corresponding values of FWHM obtained by fitting a Lorentz function.

The confocal Raman spectroscopy

The interface structure of LiTFSI electrolytes can be measured by confocal Raman spectroscopy. This technique has been reported to detect the interfacial effect between two different phases in electrolytes.[2, 3] A small KB electrode is immersed in the LiTFSI electrolyte placed on the glass slide during the Raman experiment. The schematic diagram of the different focal positions on the electrolyte with the KB electrode is showed in Figure S5a and it is easy to make the focal point focus on the KB electrode surface which it is a dark area in the confocal microscopy. Figure S5b-e show that the offset of S-N-S bending vibration of $TFSI^-$ anions and the intensity of O-H stretching vibration of H_2O with the KB electrode depends on the focal point of a confocal microscope. Figure S5b and c focus on the low wave number region which show the S-N-S bending vibration of $TFSI^-$ anions. For the pure LiTFSI electrolyte, there is a characteristic peak at 744 cm^{-1} corresponding to the S-N-S bending vibration of $TFSI^-$ anions. For the pure KB electrode sample, a characteristic peak of the defects and disordered carbon (D-band) could be found at 1350 cm^{-1}, which is induced by the disorder and defects in carbon materials.[4] No characteristic peak appears at about 745 cm^{-1} with the absence of LiTFSI electrolyte. When the focal point focuses on an area near the KB electrode surface in LiTFSI electrolyte, the characteristic peak of the S-N-S bending vibration shifts to higher wavenumbers, accompanied by the presence of the D-band from the KB electrode. When the focal point locates in the liquid phase of the LiTFSI electrolyte with the KB electrode, we find that the position of the characteristic peak of S-N-S bending vibration is nearly the same as the pure LiTFSI electrolyte and the D-band from the KB electrode almost disappears. Figure S5d and e focus on the high wave number region which reflect O-H stretching vibration of H_2O. For pure water, a broad Raman band from 3000 to 3700 cm^{-1} includes the symmetric vibration modes of O-H at about 3250 cm^{-1} and asymmetric vibration

modes of O-H at 3410 cm cm^{-1}.[5] For the pure LiTFSI electrolyte, the broad Raman spectra of O-H stretching vibration bands vanishes gradually and a sharp peak at 3560 cm^{-1} appears. This peak is attributed to the signature of crystalline hydrates, where most water molecules participate in ion coordination with cations and anions of the salt, giving rise to a unique solvation structure.[5] When the focal point focuses on an area near the KB electrode surface in LiTFSI electrolyte, the characteristic peaks of carbon materials (D-band at 1350 cm^{-1} and G-band at 1600 cm^{-1}) appears. The peak of O-H stretching vibration bands at 3560 cm^{-1} is significantly weakened compared with that in the liquid phase of the LiTFSI electrolyte (away from the interface) with the KB electrode. And this peak in the liquid phase of the LiTFSI electrolyte with the KB electrode is similar with the pure electrolytes. This result demonstrates that water molecules are expelled away from the interface, corresponding to the more solid-like LiTFSI at the interface.

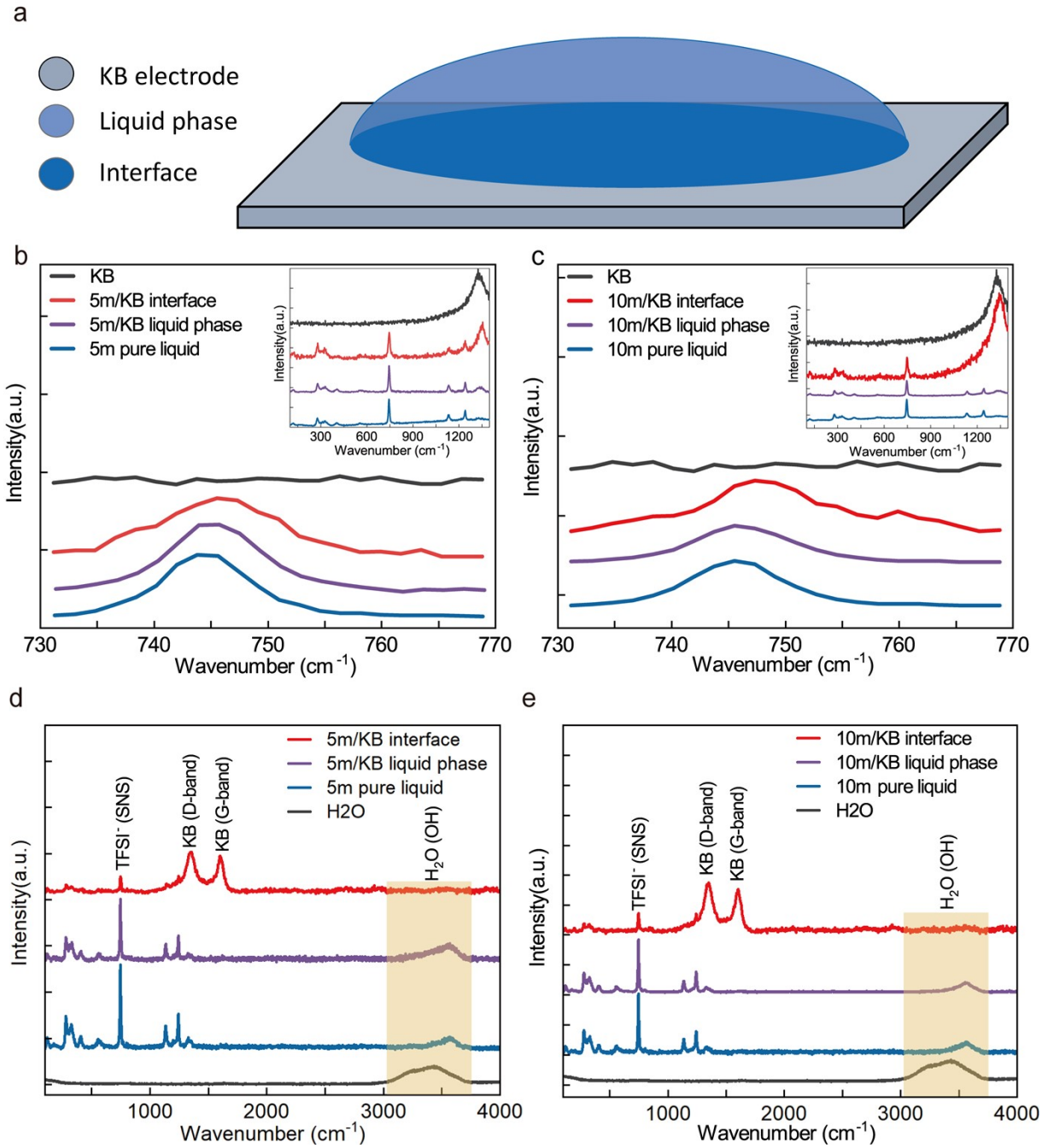

Figure S5. (a) The schematic diagram of the different focal positions on the electrolyte with the KB electrode. The confocal Raman spectra of S-N-S bending vibrations of $TFSI^-$ anions in (b) 5 m and (c) 10 m LiTFSI electrolytes. The inset shows the whole scanning region of confocal Raman spectroscopy. The characteristic peak of carbon (D-band at 1350 cm^{-1}) is found on the pure KB

electrode and the interface region near the KB electrode. The confocal Raman spectra of O-H stretching vibration bands of H_2O in (a) 5 m and (b) 10 m LiTFSI electrolytes. The yellow area is O-H stretching vibration bands of H_2O. The characteristic peaks of carbon (D-band at 1350 cm^{-1} and G-band at 1600 cm^{-1}) is found on the interface region near the KB electrode.

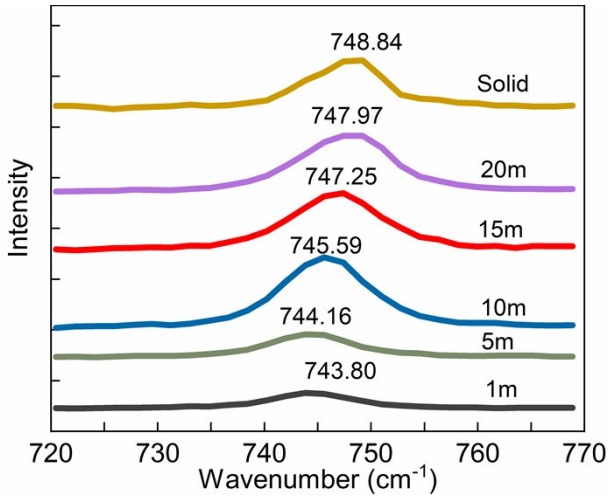

Figure S6. The confocal Raman spectra of LiTFSI electrolytes with different concentrations.

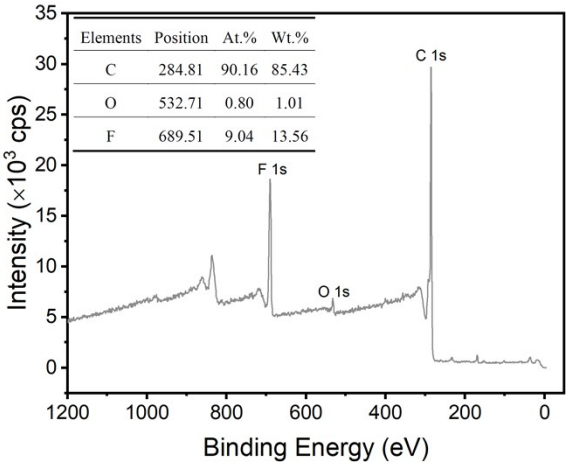

Figure S7. XPS spectrum of the KB electrode. the inset is the table of elements.

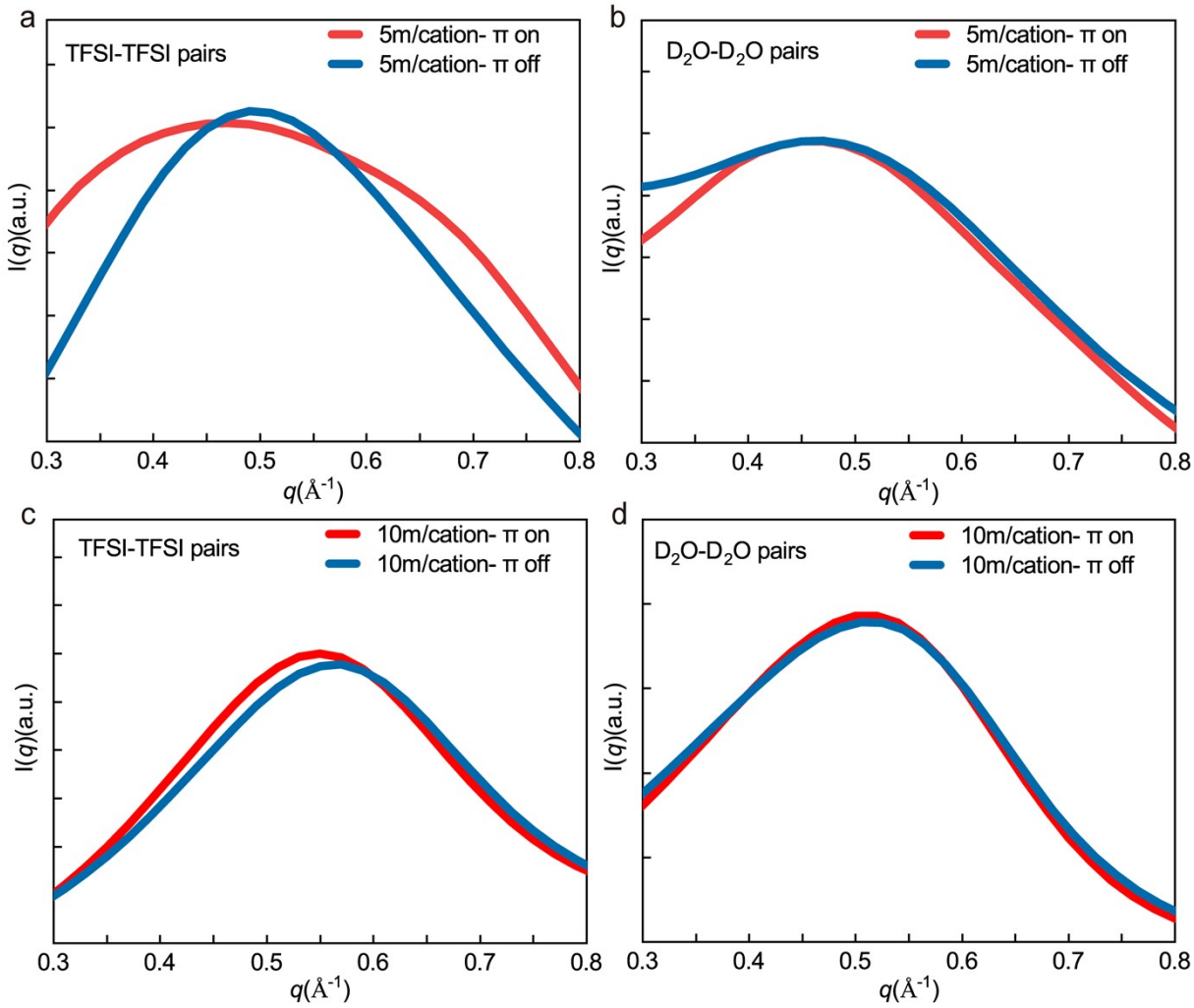

Figure S8. The partial neutron scattering profiles (PNSPs) of different pairs derived from MD simulations with Model 1. (a)$TFSI^-$−$TFSI^-$ in 5 m. (b) D_2O–D_2O in 5 m. (c) $TFSI^-$−$TFSI^-$ in 10 m. (d) D_2O–D_2O in 10 m. The red line and blue line represent the carbon electrodes with and without cation−π interactions.

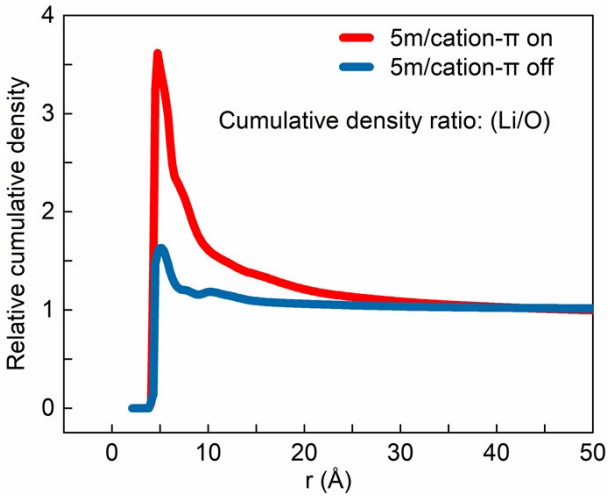

Figure S9. The ratio of the relative cumulative density for Li and O atoms of H_2O within a 1 nm distance from carbon electrodes derived from MD simulations with Model 1.

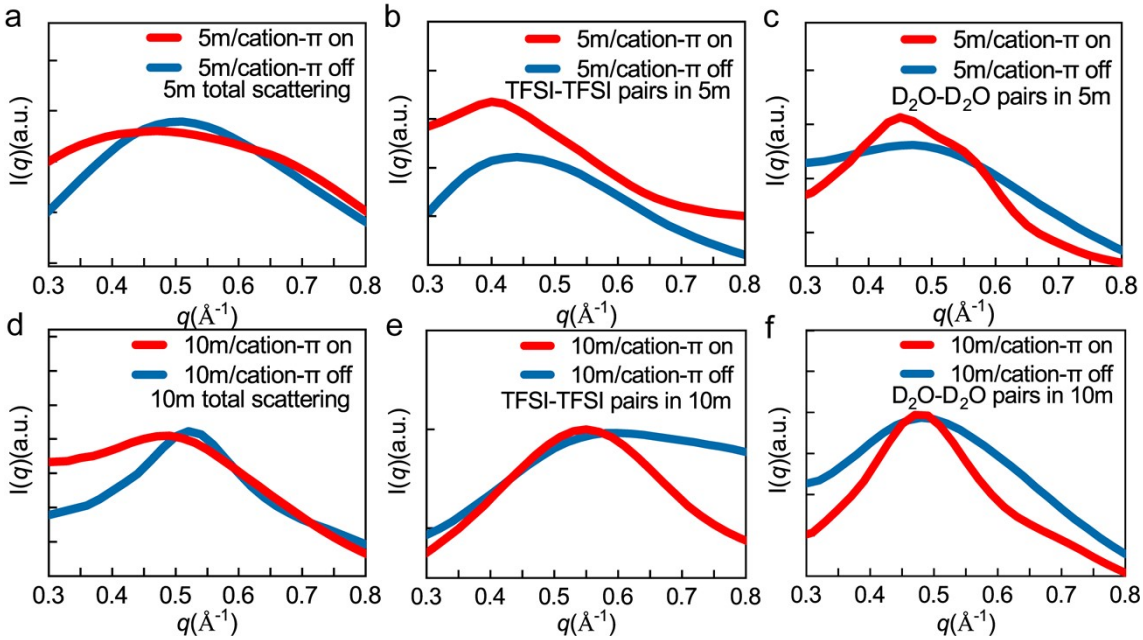

Figure S10. Neutron scattering profiles for (a) 5 m and (d) 10 m LiTFSI electrolytes and the partial neutron scattering profiles (PNSPs) of different pairs (b)$TFSI^-$–$TFSI^-$ in 5 m. (c) D_2O–D_2O in 5 m. (e) $TFSI^-$–$TFSI^-$ in 10 m. (f) D_2O–D_2O in 10 m derived from MD simulations with Model 2. The red line and blue line represent the carbon electrodes with and without cation–π interactions.

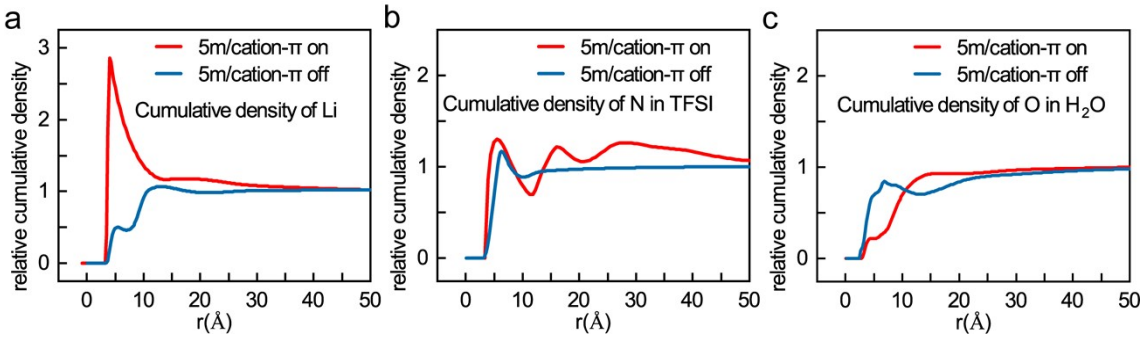

Figure S11 The relative cumulative densities normalized with that of bulk solution derived from MD simulations with Model 2: (a) Li^+, (b) N atoms of $TFSI^-$ anions, and (c) O atoms of water molecules in 5 m.

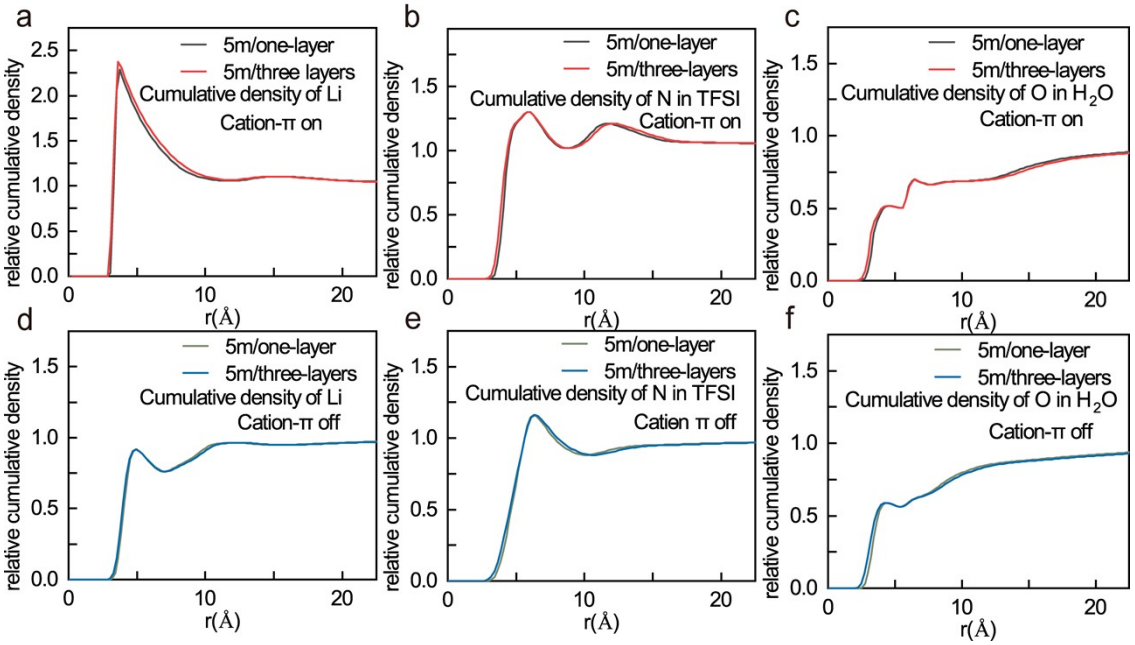

Figure S12. The relative cumulative density of each element in LiTFSI electrolyte under different graphene layers: (a) Li atoms, (b) N atoms of $TFSI^{-1}$ anions, and (c) O atoms of H_2O in 5 m with cation-π on; (d) Li atoms, (e) N atoms of TFSI anions and (f) O atoms of H_2O in 5 m with cation-π off.

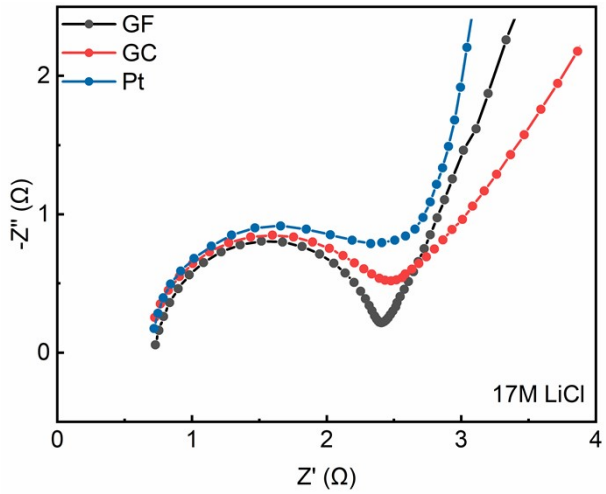

Figure S13. The Nyquist plots of 17 m LiCl electrolyte with graphite flake (GF, black), glassy carbon (GC, red), and platinum (Pt, blue) electrodes.

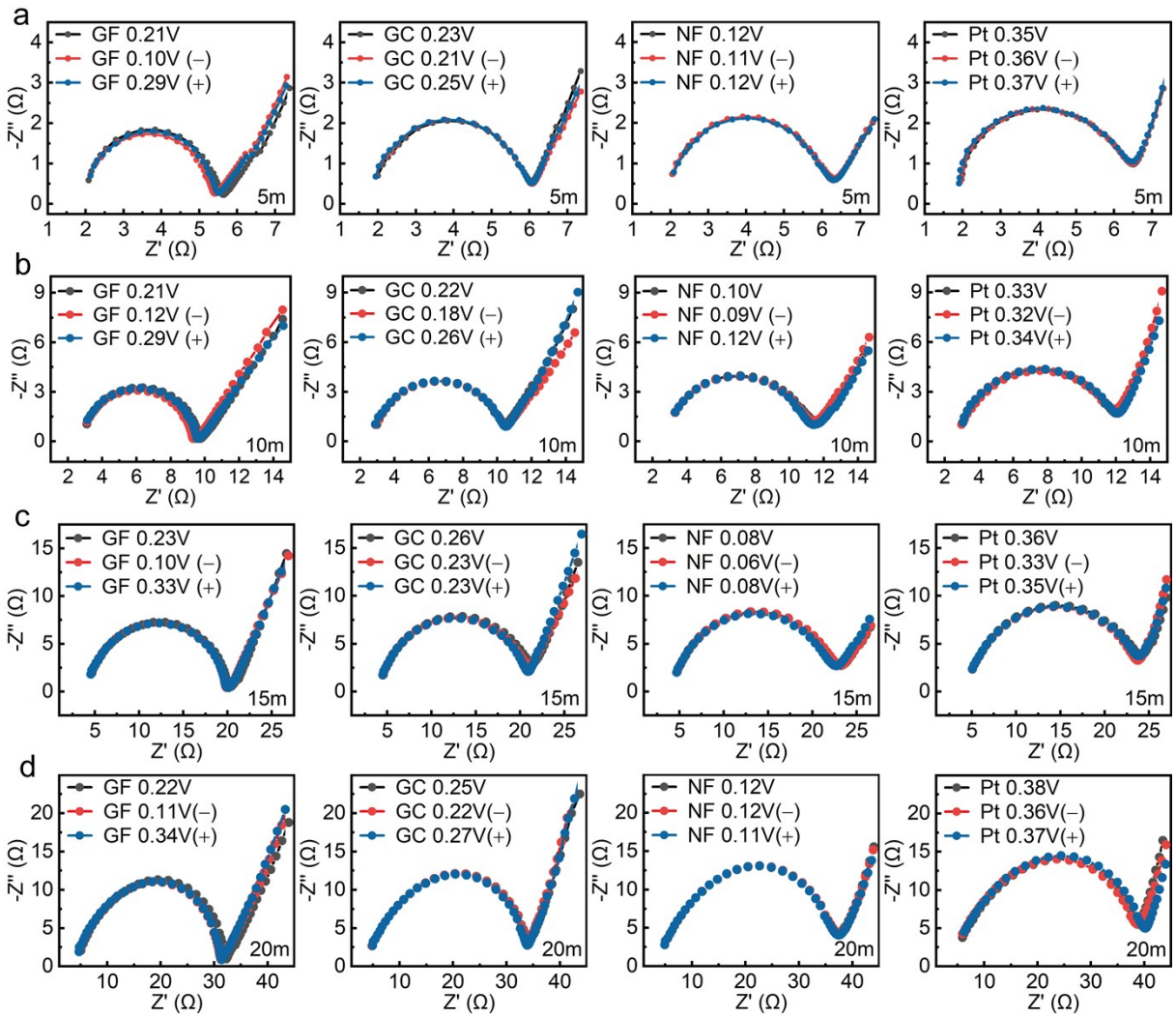

Figure S14. The Nyquist plots of different electrodes (GF, GC, NF, and Pt) in (a) 5 m, (b) 10 m, (c) 15 m, and (d) 20 m LiTFSI electrolytes with different OCVs (initial voltage (black), negative voltage (red), and positive voltage (blue)).

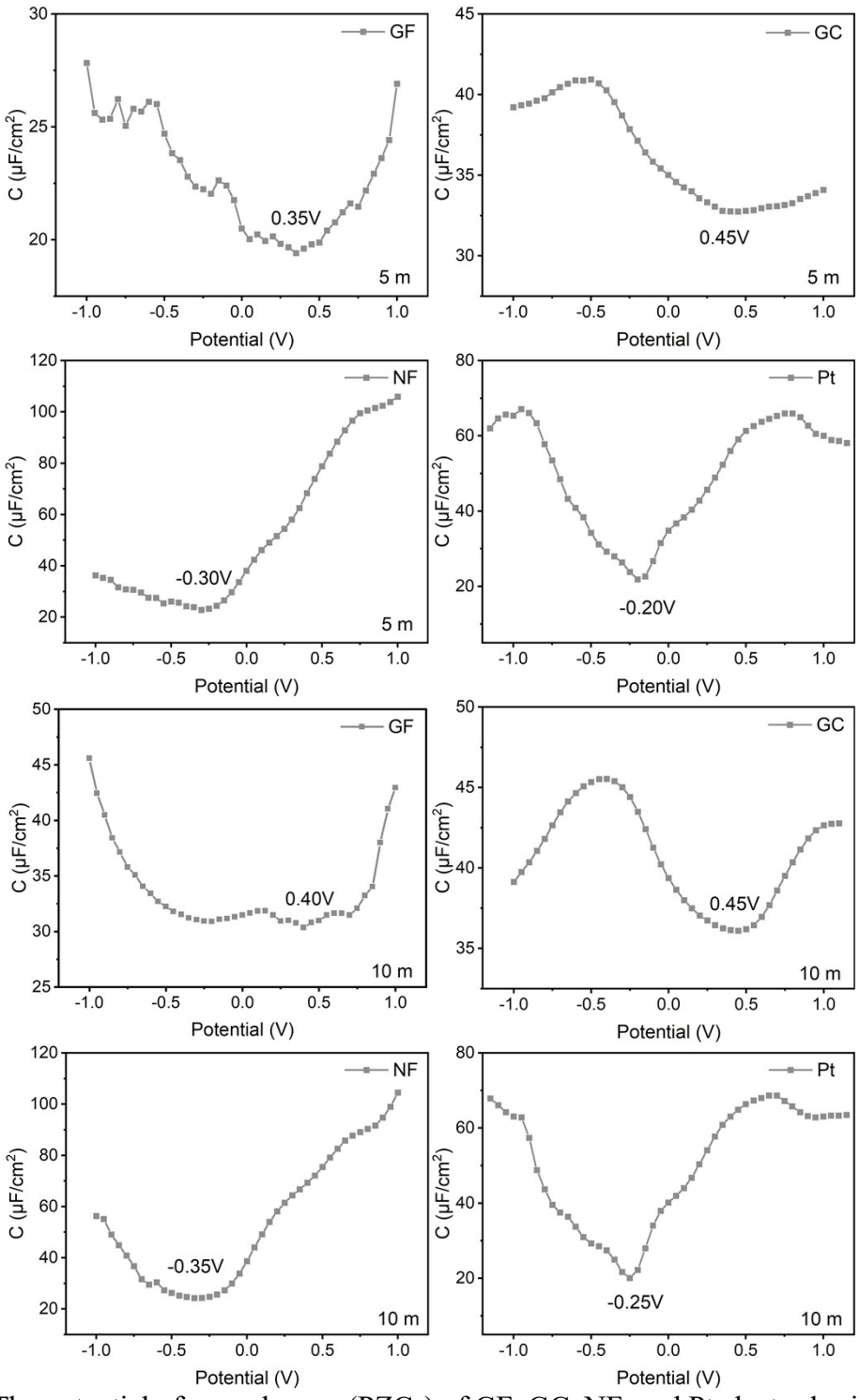

Figure S15. The potential of zero charges (PZCs) of GF, GC, NF, and Pt electrodes in 5 m and 10 m LiTFSI electrolytes.

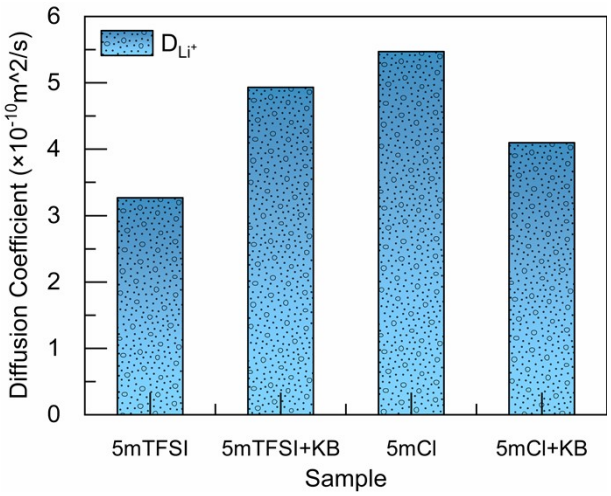

Figure S16. The diffusion coefficient of Li^+ ($^{D}_{Li^+}$) near the interface in LiTFSI and LiCl electrolytes from NMR.

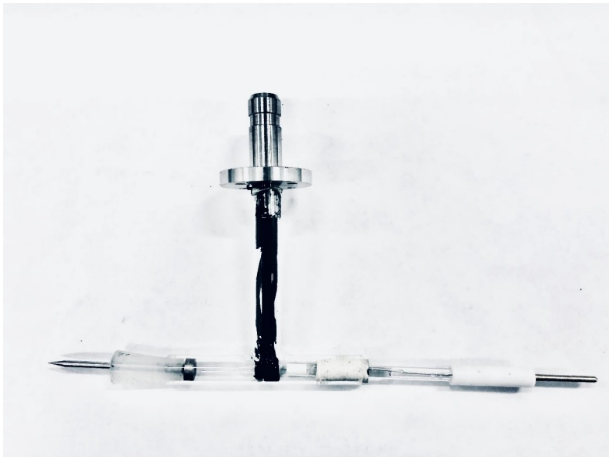

Figure S17. The experimental device of tee quartz tube for neutron diffraction.

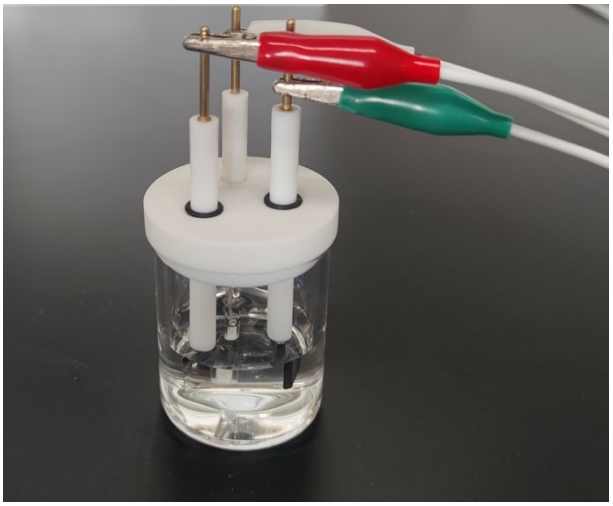

Figure S18. The experimental device of the electrochemical cell for EIS measurements.

REFERENCES

(1) Horwitz, G.; Härk, E.; Steinberg, P. Y.; Cavalcanti, L. P.; Risse, S.; Corti, H. R. The Nanostructure of Water-in-Salt Electrolytes Revisited: Effect of the Anion Size. *ACS Nano* **2021**, *15* (7), 11564-11572.

(2) Poltorak, L.; Dossot, M.; Herzog, G.; Walcarius, A. Interfacial Processes Studied by Coupling Electrochemistry at the Polarised Liquid–Liquid Interface with in Situ Confocal Raman Spectroscopy. *Phys. Chem. Chem. Phys.* **2014**, *16* (48), 26955-26962.

(3) Forster, J. D.; Harris, S. J.; Urban, J. J. Mapping Li+ Concentration and Transport Via in Situ Confocal Raman Microscopy. *J. Phys. Chem. Lett.* **2014**, *5* (11), 2007-2011.

(4) Matthews, M. J.; Pimenta, M. A.; Dresselhaus, G.; Dresselhaus, M.; Endo, M. Origin of Dispersive Effects of the Raman D Band in Carbon Materials. *Phys. Rev. B* **1999**, *59* (10), R6585.

(5) Lee, M. H.; Kim, S. J.; Chang, D.; Kim, J.; Moon, S.; Oh, K.; Park, K.-Y.; Seong, W. M.; Park, H.; Kwon, G. Toward a Low-Cost High-Voltage Sodium Aqueous Rechargeable Battery. *Materials Today* **2019**, *29*, 26-36.